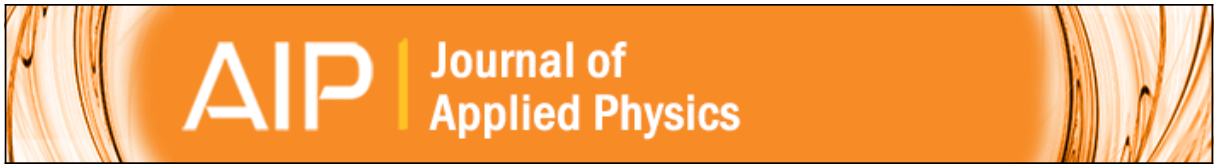

Design and fabrication of planar multilayer structures with coherent thermal emission characteristics

B. J. Lee and Z. M. Zhang

Citation: Journal of Applied Physics **100**, 063529 (2006); doi: 10.1063/1.2349472
View online: http://dx.doi.org/10.1063/1.2349472
View Table of Contents: http://scitation.aip.org/content/aip/journal/jap/100/6?ver=pdfcov
Published by the AIP Publishing

Articles you may be interested in

Far field coherent thermal emission from a bilayer structure
J. Appl. Phys. **109**, 034315 (2011); 10.1063/1.3544359

Light emission properties of planar source in multilayer structures with photonic crystal patterns
J. Appl. Phys. **108**, 063103 (2010); 10.1063/1.3483941

Coupling of surface plasmons between two silver films in a Ag / SiO 2 / Ag plasmonic thermal emitter with grating structure
Appl. Phys. Lett. **93**, 263106 (2008); 10.1063/1.3058767

Coherent thermal emission from one-dimensional photonic crystals
Appl. Phys. Lett. **87**, 071904 (2005); 10.1063/1.2010613

Ni–Cr passivation of very thin Ag films for low-emissivity multilayer coatings
J. Vac. Sci. Technol. A **17**, 3449 (1999); 10.1116/1.582081

[This article is copyrighted as indicated in the article. Reuse of AIP content is subject to the terms at: http://scitation.aip.org/termsconditions. Downloaded to] IP: 149.151.178.171 On: Thu, 24 Sep 2015 20:04:27

Design and fabrication of planar multilayer structures with coherent thermal emission characteristics

B. J. Lee and Z. M. Zhang[a)]
G.W. Woodruff School of Mechanical Engineering, Georgia Institute of Technology, Atlanta, Georgia 30332

(Received 12 March 2006; accepted 27 June 2006; published online 28 September 2006)

A large number of recent publications dealt with enhanced emission properties of micro/nanostructures by the excitation of surface plasmon or phonon polaritons. Some used grating structures to demonstrate coherent thermal emission in a narrow spectral band and towards a well-defined direction. Others suggested that planar layers could also be used to achieve coherent emission. In the present paper, we describe two alternative designs with fewer layers for the application as coherent emission sources in planar multilayer structures. One design is a composite of several unit cells of one-dimensional photonic crystal atop a highly reflective material. Coherent emission can be obtained by the excitation of surface waves between the photonic crystal and the reflector. The other design employs a Fabry-Pérot resonance cavity constructed by coating a dielectric layer onto the reflector and then a thin metallic film on the dielectric layer. When standing waves exist in the cavity, the emissivity plots show sharp spectral peaks and narrow angular lobes. By optimizing the film thicknesses, a close-to-unity emissivity can be achieved from the proposed structures. The theoretical predictions are supported by the measured spectral reflectance from fabricated samples. © *2006 American Institute of Physics*. [DOI: 10.1063/1.2349472]

I. INTRODUCTION

Thermal emission from hot objects usually exhibits broadband and quasi-isotropic features.[1] However, rapid advancement in technologies of micro/nanofabrication has enabled the control of thermal emission by modifying surface structures.[2,3] As a consequence, coherent thermal emission has recently been demonstrated from microstructured surfaces, as manifested by a sharp spectral peak in a narrow band (i.e., temporal coherence) and a narrow angular lobe into a well-defined direction (i.e., spatial coherence).[4] The development of spectrally and directionally selective emission source is crucial for improving the efficiency of energy conversion systems, such as solar cells[5] and thermophotovoltaic devices.[6] The objective of the present study is to identify and experimentally demonstrate unique structures with coherent emission characteristics.

A number of studies used surface relief gratings, made of a metal[7] or a polar material,[4] to demonstrate coherent thermal emission. For grating structures, coherence features of thermal emission are primarily associated with the excitation of surface plasmon (for metal) or surface phonon (for polar material) polaritons, which can be directly coupled to propagating waves in air due to diffractions by the periodic gratings. To excite surface waves from gratings, a magnetic field component parallel to the grating grooves is required. Such a magnetic field component exists in one or both of the transverse magnetic (TM) and transverse electric (TE) waves depending on the direction of emission. In the case when the direction of emission is perpendicular to the grooves, coherent emission is restricted to TM waves. A magnetic material with a negative permeability can be used to excite surface waves for TE waves.[8] While metamaterials with a negative permeability has been experimentally demonstrated in the microwave spectral region,[9] these materials have not been fabricated for the near-infrared (IR) and mid-IR spectral regions, where thermal radiation mainly occurs.[1]

Coherent thermal emission sources have also been proposed from planar multilayer structures.[10–19] In particular, considerable enhancement of thermal emission is achieved via two mechanisms: excitation of surface waves or wave interference effects. Previously, it has been shown that surface waves can be excited at the interface between a semi-infinite one-dimensional (1D) photonic crystal (PC) and a metal[20] or a polar material[11,12] without using a prism. Since the surface wave is nonradiative,[8] attenuated total reflection (ATR) configuration is often used to excite surface waves between the 1D PC and dielectrics.[21] Similar to grating structures, the excited surface waves enable coherent thermal emission from the structure made of a thin SiC layer coated on the semi-infinite PC for both polarizations.[22,23] This is because an *effective* evanescent wave, which is an oscillating field with a decaying amplitude, exists inside the PC in the stop band regardless of the polarization.[11,12] A recent study has shown that a truncated two-dimensional (2D) PC can also generate coherent thermal emission in the stop band.[24] Another type of coherent emission source is based on the wave interference effects, such as in a semitransparent layer[14] or a Fabry-Pérot cavity resonator with highly reflective coatings.[13,16,17] The reflectors can be made by using a metallic layer, doped silicon, or a Bragg mirror, which is a special case of 1D PC. Coherent thermal emission from the resonance cavity can also occur for both polarizations due to wave interference effects. Furthermore, coherent characteristics of thermal emission can be found from a 2D microcavity[25] or a three-dimensional (3D) PC (Ref. 26)

[a)]Electronic mail: zzhang@mail.me.gatech.edu

 © 2006 American Institute of Physics

[This article is copyrighted as indicated in the article. Reuse of AIP content is subject to the terms at: http://scitation.aip.org/termsconditions. Downloaded to] IP: 149.151.178.171 On: Thu, 24 Sep 2015 20:04:27

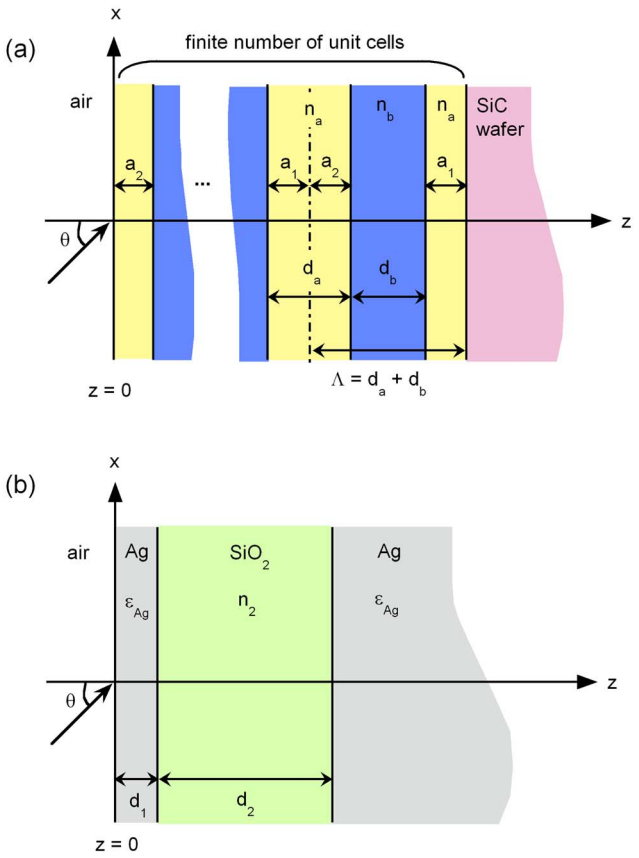

FIG. 1. (Color online) Schematics of the proposed coherent emission sources: (a) a PC-on-SiC structure made of a 1D PC with few unit cells coated on the SiC wafer. The unit cell of the 1D PC is composed of a dielectric type a on both sides of a dielectric type b with a total thickness of $\Lambda=d_a+d_b$, where $d_a=a_1+a_2$. The thickness a_1 determines the surface termination of the PC adjacent to the SiC wafer. (b) Asymmetric Fabry-Pérot resonance cavity made of a SiO_2 film with Ag coatings on both sides. The thickness of the Ag layer located on the left is d_1, and that on the right is assumed to be semi-infinite.

made of tungsten; however, the fabrication of these structures is more complicated than 1D planar structures.

We have designed, fabricated, and tested two alternative planar multilayer structures as coherent thermal emission sources that exhibit both temporal and spatial coherences. One structure involves the 1D PC with finite number of unit cells on a polar material, such as SiC, and is illustrated in Fig. 1(a). Hereafter, it will be called as the PC-on-SiC structure. The unit cell of the 1D PC is composed of alternating dielectrics with different refractive indices n_a and n_b, and is defined by the thicknesses: a_1, d_b, and a_2, where $a_1+a_2=d_a$ with a period of $\Lambda=d_a+d_b$. The thickness a_1 determines the surface termination of the 1D PC adjacent to SiC. Even though the employed PC is not semi-infinite and consists of several unit cells only, evanescent waves can exist inside the truncated PC in the stop band. Hence, surface waves are supported at the interface between the 1D PC and SiC. Compared to the previous structure, where a thin SiC film is coated on the semi-infinite 1D PC,[11,12] the PC-on-SiC structure requires far fewer layers and, thus, is much easier to manufacture.

The other structure is an asymmetric Fabry-Pérot resonance cavity made of a dielectric layer with highly reflective coatings on both sides, as shown in Fig. 1(b). Although similar structures were considered by others,[27,28] the spectral emission peaks are too broad without sharp angular lobes. By using highly reflective materials on both sides of the dielectric layer, the present study demonstrates both temporal and spatial coherences in the mid- and near-IR spectral regions. Furthermore, conditions that influence coherent emission characteristics from both proposed structures are investigated. The band structure of the truncated PC is analyzed by comparing it with that of the semi-infinite PC. Based on the calculated results, the proposed structures were designed and built using thin-film deposition techniques. The spectral reflectance was measured at near normal incidence with a Fourier transform infrared (FTIR) spectrometer, and the measured reflectance confirms the theoretical prediction.

II. REFLECTANCE OF TRUNCATED PHOTONIC CRYSTALS

A 1D PC is a periodic multilayer structure, whose unit cell is composed of alternating dielectrics with different refractive indices. Without loss of a generality, it is assumed that each layer is perpendicular to the z axis, as shown in Fig. 1. Due to the periodicity in optical constants of each layer, the electromagnetic wave inside the PC must satisfy the Bloch wave condition in the z direction, similar to the wave function of electrons in crystalline structures.[29] Hence, the electric field vector in the 1D PC can be expressed in the Bloch wave form,

$$\boldsymbol{E}(x,y,z,t)=\boldsymbol{u}(z)e^{iKz}e^{i(k_x x+k_y y-\omega t)}, \tag{1}$$

where $\boldsymbol{u}(z+\Lambda)=\boldsymbol{u}(z)$ is a periodic function of z with a period Λ that is nothing but the lattice constant of the PC, K is the Bloch wave vector, k_x and k_y are the parallel components of the wave vector that must be the same in all layers as required by the phase matching conditions, and ω is the angular frequency. In general, the Bloch wave vector K is a complex quantity and becomes a scalar for the 1D PC. Due to the axial symmetry of the planar structure, the coordinate can always be rotated around the z axis to ensure that $k_y=0$. For TE wave, where the electric vector is perpendicular to the x-z plane, the Bloch condition described in Eq. (1) requires that the nonzero component of the electric field vector satisfies the following condition:

$$E_y(x,y,z+\Lambda,t)=E_y(x,y,z,t)e^{iK\Lambda}. \tag{2}$$

In other words, the ratio of the electric fields at two points separated by Λ in the z direction is equal to $e^{iK\Lambda}$. On the other hand, the electric field should also satisfy Maxwell's equations. For 1D case, the solution of Maxwell's equations can be obtained by using the transfer matrix formulation described in detail elsewhere.[30,31] By comparing Eq. (2) with the solution obtained from the matrix formulation, K can be solved for given material properties and geometry.[12]

The band structure of the 1D PC can be constructed from the Bloch wave vector.[22] Consider a semi-infinite PC located in the positive-z half plane starting at $z=0$. The electric field propagates infinitely into the PC if $\mathrm{Im}(K)=0$. The region where K becomes real in the $\omega-k_x$ domain is called a pass-

[This article is copyrighted as indicated in the article. Reuse of AIP content is subject to the terms at: http://scitation.aip.org/termsconditions. Downloaded to] IP: 149.151.178.171 On: Thu, 24 Sep 2015 20:04:27

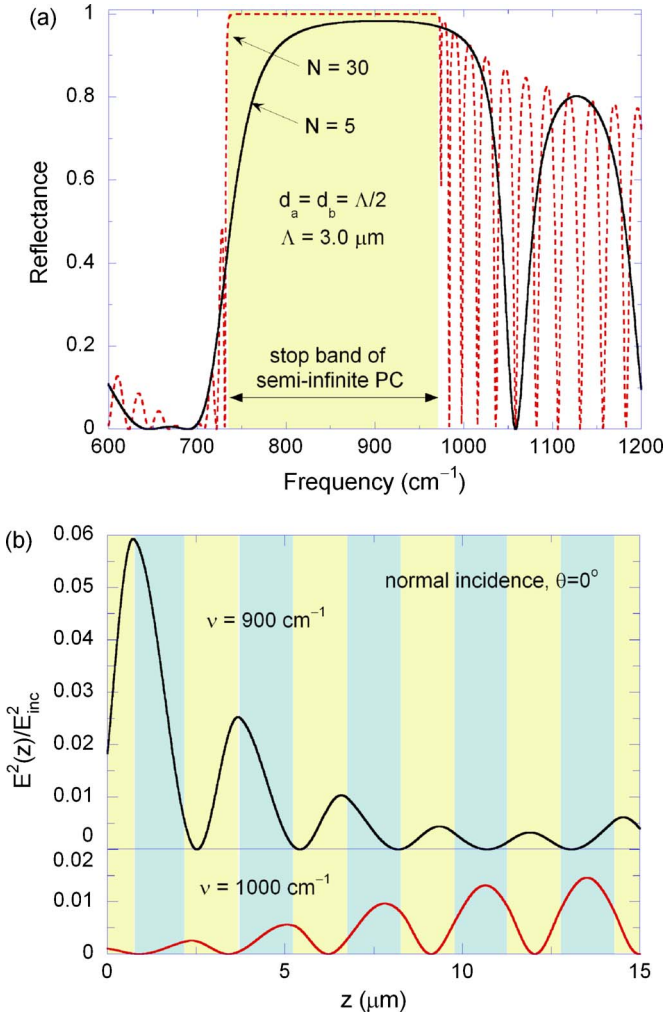

FIG. 2. (Color online) Characteristics of PCs of finite numbers of periods: (a) reflectance spectra in the vicinity of the stop band. The solid line stands for the case when $N=5$, i.e., five unit cells, and the dotted line is for the case with $N=30$. The stop band of the semi-infinite 1D PC is represented by the shaded region. (b) The square of the electric field, normalized by that of the incident wave, inside the PC for $N=5$ at normal incidence. The upper panel is for the case of $\nu=900\ \mathrm{cm}^{-1}$ (stop band), and the lower panel is for $\nu=1000\ \mathrm{cm}^{-1}$ (passband).

band. On the other hand, when $\mathrm{Im}(K)\neq 0$, the amplitude of Bloch wave is decaying exponentially into the positive-z direction and, thus, the electric field is localized near the surface at $z=0$. The region where $\mathrm{Im}(K)\neq 0$ is called a stop band, in which the electric field is evanescent inside the PC. From the band structure of the PC, one can observe alternating passband and stop band in the $\omega-k_x$ domain, similar to the energy band of electrons. In general, the reflectance of such a semi-infinite 1D PC is unity at the stop band because no energy can penetrate into the PC. Since the proposed structure employs the truncated 1D PC, a brief discussion about the effect of the number of unit cells on the band structure is presented next.

Figure 2(a) shows the reflectance spectra of PCs at normal incidence in the vicinity of a stop band. The dotted line represents the reflectance of a PC with 30 unit cells ($N=30$), and the solid line is for a PC with five unit cells ($N=5$). The shaded region stands for the stop band of the semi-infinite PC obtained by solving the Bloch wave vector based on the transfer matrix formulation.[12] In the calculation, constituent dielectrics a and b are chosen as ZnSe and KBr, whose refractive indices are approximately $n_a=2.4$ and $n_b=1.5$, respectively,[32] and the thicknesses of dielectrics are set to be $d_a=d_b=\Lambda/2$. Here, the unit cell is taken as the symmetric three-layer structure consisting of a dielectric a on both side of a dielectric b and, thus, the thickness a_1, defined in Fig. 1(a), is equal to $d_a/2$. The stop band of the PC is scaled by changing Λ to approximately match the SiC phonon absorption band that appears in the mid-IR region at frequencies (ν) from 793 to 969 cm^{-1}. In the present paper, the frequency is in cm^{-1}. Consequently, the period $\Lambda=3\ \mu$m is selected for the use in Fig. 2(a). From the reflectance spectrum, the stop band of the PC with $N=30$ can be thought as the spectral region where the reflectance becomes unity. It is clear that $N=30$ is sufficient to be approximated as the semi-infinite 1D PC in the stop band. Note that interference effects cause some oscillations in the reflectance spectrum at the frequency regions lower than 730 cm^{-1} and higher than 970 cm^{-1}, i.e., in passbands. The period of oscillation varies with the number of unit cells. The reduction in the reflectance is associated with an increase in the transmittance through the finite-thickness PC. Since PCs can support surface waves in the stop band,[29] features in the stop band are the main focus of the present study.

For $N=5$, although the band edge is not well defined in the reflectance spectrum, the stop band still exists in the region where the reflectance is close to unity. This is clear from the fact that the spectral band of large reflectance is much wider in the stop band than that normally found in the passband due to interference effects. Interestingly, the stop band of the PC with $N=5$ appears shifted a little towards higher frequencies, compared to that of the semi-infinite PC. This is caused by interference effects as explained below. The square of the electric field, normalized to that of the incidence, is plotted inside the PC with $N=5$ at normal incidence, in Fig. 2(b). Here, $E(z)$ is the real part of the complex electric field vector. The upper panel is the case for $\nu=900\ \mathrm{cm}^{-1}$ (in the stop band), and the lower panel is for $\nu=1000\ \mathrm{cm}^{-1}$ (in the passband). It can be seen from Fig. 2(a) that reflectance values are greater than 0.9 for both cases. In terms of the field distribution in Fig. 2(b), the upper panel clearly shows the effective evanescent wave, which is an oscillating field with exponentially decaying amplitude as z approaches infinity. In a semi-infinite PC, the effective evanescent wave does not carry energy; thus no energy can transmit through a semi-infinite PC in the stop band even though an oscillating field exists inside the PC. On the other hand, the small number of periods does not guarantee zero transmission at $\nu=900\ \mathrm{cm}^{-1}$. In fact, the field seems to increase somehow near $z=15\ \mu$m. Therefore, the reflectance in the stop band of the truncated PC is generally less than unity. The lower panel of Fig. 2(b) shows that the amplitude of the electric field for $\nu=1000\ \mathrm{cm}^{-1}$ is rather amplifying from $z=0$ to 15 μm, suggesting that the field distribution is actually a part of the Bloch wave, which propagates through the PC in the passband. At $z=15\ \mu$m, the field amplitude is very

[This article is copyrighted as indicated in the article. Reuse of AIP content is subject to the terms at: http://scitation.aip.org/termsconditions. Downloaded to] IP: 149.151.178.171 On: Thu, 24 Sep 2015 20:04:27

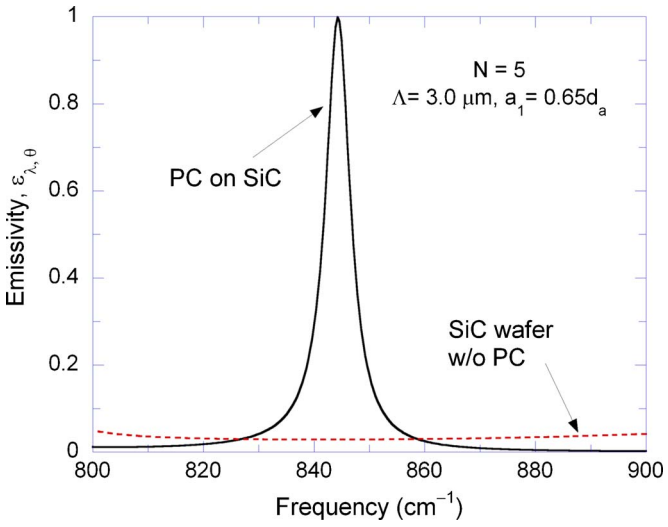

FIG. 3. (Color online) The spectral-directional emissivity $\varepsilon_{\lambda,\theta}$ of the PC-on-SiC structure at normal incidence (solid line). The parameters of the 1D PC are $\Lambda=3$ μm, $N=5$, $d_a=d_b=\Lambda/2$, and $a_1=0.65d_a$. The dotted line represents the emissivity of a bulk SiC wafer without the 1D PC.

small so that the transmittance is very low. In other words, the high reflectance at $\nu=1000$ cm^{-1} is due to interference effects.

III. PREDICTION OF COHERENT THERMAL EMISSION

The analysis of coherent thermal emission from multilayer structures is presented in the following using either a modified photonic crystal or a Fabry-Pérot cavity structure.

A. Modified photonic crystal

A surface wave is an electromagnetic wave that propagates along the interface and decays exponentially from the interface into both media.[8] In order to excite the surface wave, evanescent waves are required in both media. In addition, for homogenous materials, the electric permittivities (for TM waves) or magnetic permeabilities (for TE waves) should be of opposite signs in order to excite the surface wave. Notice that effective evanescent waves exist for both polarizations in the stop bands of PCs regardless of the angle of incidence or emission angle when emission rather than absorption is considered. Furthermore, it has been shown that a PC can support surface waves in the stop band.[12,22,29] Therefore, a 1D PC is used in the present study to directly couple propagating waves from air in the left half space (i.e., $z<0$; see Fig. 1) to the surface wave. Here, the optical properties of air are assumed to be the same as those of vacuum. Although it is inappropriate to define equivalent ε and μ of the PC by regarding it as a homogeneous medium, the dispersion relation of surface waves involving a 1D PC can be derived by using the equivalent layer method[20] or supercell method.[33]

The normal emissivity of the PC-on-SiC structure is plotted in Fig. 3. The emissivity of the semi-infinite SiC wafer without a 1D PC is also plotted for comparison. Because the SiC layer is thick enough to be opaque in the region of interest, the spectral-directional absorptance of multilayer structures is calculated from $1-R$, where R is the reflectance. The emissivity is equal to the absorptivity based on Kirchhoff's law.[1] Notice that SiC is a polar material with a strong lattice absorption in the frequency region between 793 and 969 cm^{-1}. In the IR spectral region, the dielectric function (or relative electric permittivity) of SiC can be calculated from the functional expression given in the Ref. 32. In the phonon absorption band, the wave inside the SiC is evanescent because the real part of the dielectric function of SiC is negative and the imaginary part is much smaller than unity. Therefore, surface wave can be excited in the phonon absorption band of SiC. In the calculation, the PCs with five unit cells are used with the following geometric parameters: $d_a=d_b$, $\Lambda=3.0\mu$ m, and $a_1=0.65d_a$. The thickness a_1, which varies from 0 to d_a, determines the surface termination of the PC at the interface with SiC and plays an important role in tuning the coherent emission frequency as well as the peak emissivity value.[12] More detailed discussion about the surface termination effects on the emission characteristics can be found in the Refs. 33 and 34. As shown in Fig. 3, a close-to-unity emissivity peak can be achieved by employing the truncated 1D PC on top of the SiC wafer due to the excitation of surface waves. On the other hand, the emissivity of a bulk SiC without PC is very low (less than 0.1), and the corresponding reflectance is very high, which is commonly observed in the phonon absorption band of SiC.

The temporal coherence of thermal emission can be represented by the sharp spectral peak. Comparing to the previous structure, where a thin SiC film is coated on the semi-infinite 1D PC,[11,12] the PC-on-SiC structure also shows very sharp spectral peaks in the emissivity spectrum. A measure of the sharpness of emissivity peaks is the quality factor defined by $Q=\nu_c/\delta\nu$, where ν_c is the frequency corresponding to the emissivity peak and $\delta\nu$ is the full width at half maximum (FWHM). The corresponding quality factor of the emissivity peak at normal incidence is approximately 133, which is slightly lower than 230 from the previous studies using a SiC film on 30 periods of PCs.[11,12]

The major advantage of the PC-on-SiC structure over the previous work is the use of PCs with fewer unit cells. In the PC-on-SiC structure, induced evanescent waves at $z=0$ in the stop band should be able to reach the interface with SiC to excite surface waves. For this reason, care should be taken when determining the number of unit cells for the truncated 1D PC. As illustrated in Fig. 2(a), the finite-thickness PC asymptotically shows the stop bands in terms of the reflectance spectrum. As the number of periods N increases, the reflectance in the stop band reaches unity, and the band edge becomes more obvious. It should be noted that if the reflectance is less than unity in the stop band, then some portion of incident energy propagates into the PC, and the wave inside the PC starts to lose evanescent characteristics. Therefore, the number of periods must be sufficiently large, so that the finite-thickness PC properly shows the stop band. On the other hand, the effective evanescent wave, which is coupled to propagating waves in air, is localized near the surface at $z=0$.[29] In general, an electric field inside a slab can be thought of as a summation of the forward (propagating or decaying to the positive-z direction) and backward (propa-

[This article is copyrighted as indicated in the article. Reuse of AIP content is subject to the terms at: http://scitation.aip.org/termsconditions. Downloaded to] IP: 149.151.178.171 On: Thu, 24 Sep 2015 20:04:27

gating or decaying to the negative-z direction) waves. If N is too large, forward evanescent waves decaying from $z=0$ cannot reach the right surface of the finite-thickness PC. In this case, surface waves cannot be supported because no backward evanescent wave exists at the interface between the 1D PC and SiC. Notice that the surface wave at the PC-SiC interface is associated with the backward evanescent wave in the PC. Consequently, the number of periods must be optimized to enable surface waves at the interface between the 1D PC and SiC. For the proposed PC-on-SiC structure, calculations show that the optimal N is five for coherent thermal emission.

In order to change the coherent emission frequency into longer frequency regions, other polar materials, such as boron carbide (BC) and boron nitride (BN), can be used in place of SiC. Furthermore, gold (Au) or silver (Ag) films can also be used to tune thermal emission into the near-IR or visible range. In terms of the frequency tuning, metals have advantage over polar materials because most of metals have plasma frequency in the ultraviolet region. Thus, there exist evanescent waves in metals in the wide near-IR region. Remember that the spectral region for the stop band of PCs can be easily modified by scaling the period. To demonstrate the feasibility, Ag is selected to replace SiC in the present study. The optical constants of Ag are taken from the tabulated values.[32] Notice that a Ag film can be deposited on a suitable substrate, such as a silicon wafer, and it can be treated as a semi-infinite medium when its thickness exceeds about 200 nm (i.e., much greater than the radiation penetration depth).

Figure 4(a) shows the spectral-directional emissivity of the PC-on-Ag structure at $\theta=0^{\circ}$, 30°, and 60° for both polarizations. In order to locate the stop band in the near-IR spectral region, the period of the 1D PC is scaled to $\Lambda=300$ nm. The constituent dielectrics of the PC are chosen as Si_3N_4 and SiO_2, whose refractive indices are approximately $n_a=2.0$ and $n_b=1.45$, respectively, in the considered spectral region.[32] For simplicity, the thickness of two dielectrics are assumed to be the same $d_a=d_b$, and the thickness a_1 is found to be $0.6d_a$ that will maximize the emissivity peak values for TE waves. In the calculation, six unit cells are required to optimize the emissivity from the PC-on-Ag structure. With the given geometric parameters, the emissivity peak values are very high, except in the case of TM wave at $\theta=60^{\circ}$, which is close to 0.3. For TE waves, as an example, very sharp emissivity peaks are found in a narrow spectral band centered at $\nu_c=10\,232$, 10 718, and 11 940 cm^{-1} for emission angles of $\theta=0^{\circ}$, 30°, and 60°, respectively. The corresponding quality factors of the emissivity peaks are 99, 124, and 208 for $\theta=0^{\circ}$, 30°, and 60°, respectively, and these values are comparable to those from previous studies.[4,10,12] Notice that wave interference effects cause some oscillations in the passband, but resulting emissivity values are very small compared to those due to the surface wave excitation in the stop band.

The angular distribution of the spectral-directional emissivity from the PC-on-Ag structure is plotted in Fig. 4(b) at three peak frequencies for TE waves. The spatial coherence of thermal emission is apparent from the high directionality

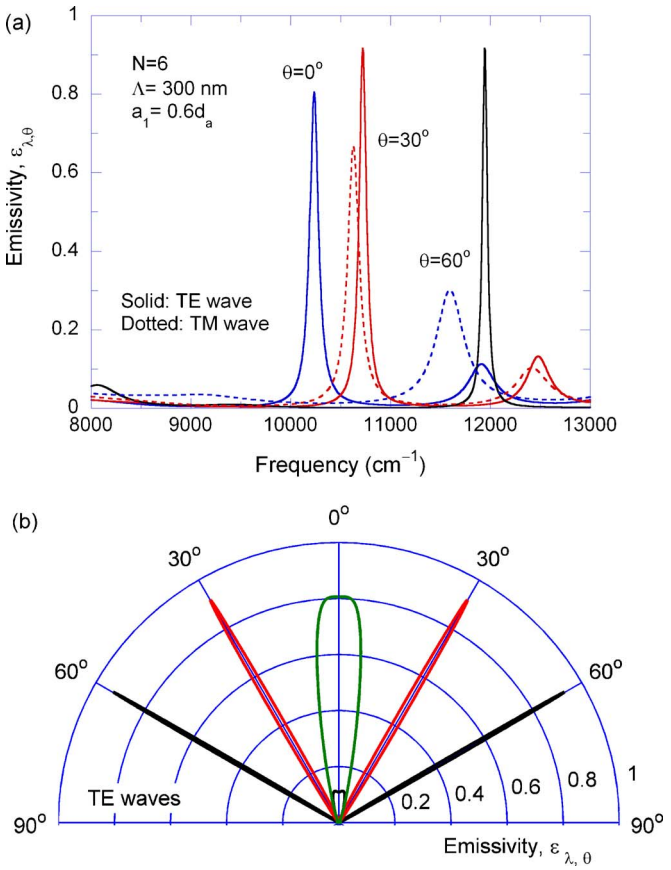

FIG. 4. (Color online) The emissivity $\varepsilon_{\lambda,\theta}$ of the PC-on-Ag structure: (a) spectral emissivity at $\theta=0°$, 30°, and 60° for TE waves (solid lines) and TM waves (dotted lines). Here, $\Lambda=300$ nm, $N=6$, $d_a=d_b=\Lambda/2$, and $a_1=0.6d_a$. (b) Angular distribution of the emissivity at three peak frequencies for TE waves. The emissivity peaks corresponding to emission angles of $\theta=0°$, 30°, and 60° are centered at $\nu_c=10\,232$, 10 718, and 11 940 cm^{-1}, respectively.

in the plot. For TE waves, the FWHMs $\delta\theta$ are estimated as 19.43°, 2.77°, and 1.35° for emission angles of $\theta=0^{\circ}$, 30°, and 60°, respectively. Except for the normal direction, excellent directionality of thermal emission is found for TE waves. Although it is not shown, the angular distribution of the emissivity for TM waves is very similar at corresponding peak frequencies except for $\theta=60^{\circ}$, where the peak emissivity is only 0.3. Notice that the thickness a_1 affects emissivity peak values and, thus, it can be tuned to maximize the emissivity at $\theta=60^{\circ}$ for TM wave. However, for Figs. 4(a) and 4(b), the thickness a_1 has been set as $0.6d_a$ by optimizing the emissivity for TE waves, which results in the close-to-unity emissivity at $\theta=30^{\circ}$ and 60° for TE wave and lower emission peaks at other conditions.

In order to ascertain that surface waves are excited at the interface between the truncated 1D PC and Ag, the square of the normalized electric field inside the PC-on-Ag structure is plotted in Fig. 5 at normal incidence. The upper panel corresponds to $\nu=10\,232$ cm^{-1} where the large emissivity peak is found, and the lower panel is for $\nu=9000$ cm^{-1} where the corresponding emissivity is less than 0.01. Here, evanescent waves are expected inside the PC for both frequencies because they correspond to the stop band. It is clear that the lower panel mainly shows forward evanescent waves coupled to propagating waves incident from air. The square

[This article is copyrighted as indicated in the article. Reuse of AIP content is subject to the terms at: http://scitation.aip.org/termsconditions. Downloaded to] IP: 149.151.178.171 On: Thu, 24 Sep 2015 20:04:27

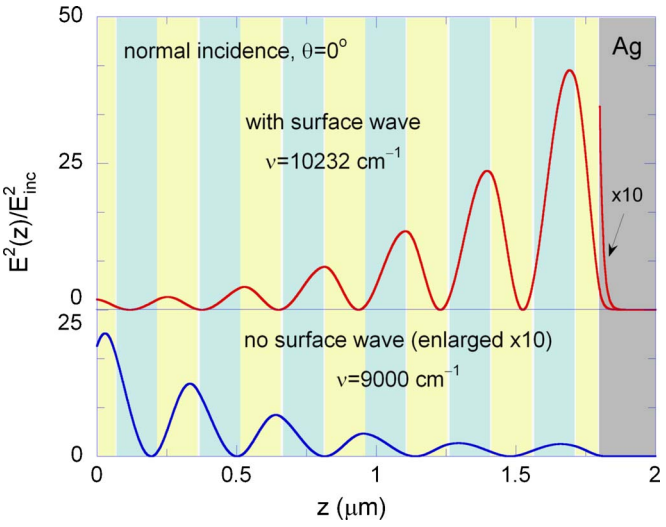

FIG. 5. (Color online) The square of the electric field, normalized by that of the incidence, inside the PC-on-Ag structure. The upper panel represents the case when a surface wave is excited, and the lower panel is for the case without a surface wave.

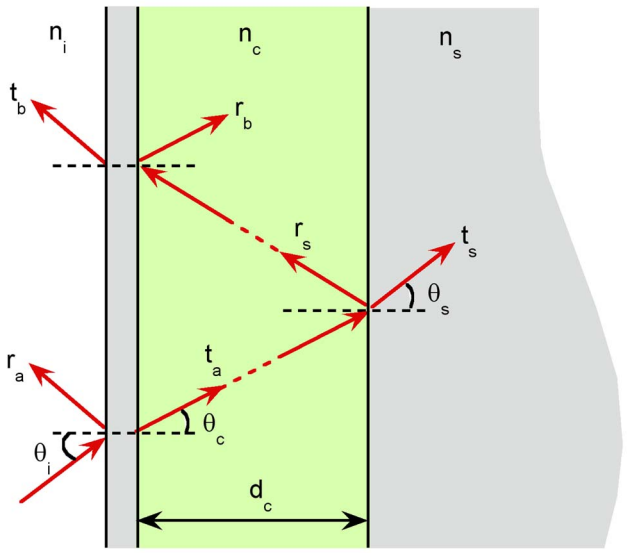

FIG. 6. (Color online) Illustration of the Fresnel reflection and transmission coefficients at the boundaries of the Fabry-Pérot resonator.

of the electric field in the lower panel is enlarged by factor of 10 for clear illustration. Since the total thickness of the PC with $N=5$ is relatively thick, backward evanescent waves reflected from the right surface of the PC are negligible compared to forward evanescent waves. On the other hand, backward evanescent waves are dominant for the upper panel. This is because surface waves are excited at the interface between the 1D PC and Ag. When surface waves are excited, evanescent waves associated with the surface wave decay from the PC-Ag interface into both media, and the electric fields inside the media are greatly enhanced due to resonance features of the surface wave. Therefore, it is natural that backward evanescent waves associated with the surface wave are dominant in the 1D PC. Because the radiation penetration depth of Ag is very small compared to the length scale of the 1D PC, the square of the electric field in the Ag layer is multiplied by 10 to clearly illustrate the exponentially decaying field inside it. It should be noted that when surface waves are excited, the incident energy is resonantly transferred to the Ag layer, resulting in a large emissivity at the resonance frequency. The maximum of the electric field is slightly off from the interface between the 1D PC and Ag, which has been also observed previously.[11,21] This could be explained as due to the nature of the effective or oscillating evanescent wave. Based on the field distribution and considerable enhancement of the field strength, it can be concluded that the surfaces waves are certainly excited at the interface between the 1D PC and Ag at $\nu=10\,232$ cm^{-1}.

B. Asymmetric Fabry-Pérot resonance cavity

An alternative design of the coherent thermal emission source is an asymmetric Fabry-Pérot resonance cavity, as shown in Fig. 1(b). Unlike the conventional Fabry-Pérot resonator made of two parallel reflectors separated by at a finite distance, the proposed structure employs a dielectric film coated with highly reflective materials of different thicknesses. Here, "asymmetric" emphasizes that the geometry of reflectors is not symmetric with respect to the cavity in the proposed structure. In general, high reflection from the boundaries of the resonance cavity is essential for the sharp spectral peak at the resonance condition.[35] In the present study, we employed SiO_2 to form the cavity and Ag as the reflective coating.

Figure 6 illustrates the reflection and transmission coefficients at the boundaries of the resonance cavity. Based on Airy's formulas, the reflection and transmission coefficients of the Fabry-Pérot cavity are expressed in the form of a superposition of amplitudes of fields,[30,31]

$$r = r_a + \frac{t_a t_b r_s e^{i2\beta}}{1 - r_b r_s e^{i2\beta}}, \tag{3}$$

$$t = \frac{t_a t_s e^{i\beta}}{1 - r_b r_s e^{i2\beta}}, \tag{4}$$

where $\beta=2\pi n_c d_c \cos\theta_c/\lambda$ is the phase shift upon traveling inside the cavity with the refractive index n_c and the thickness d_c. Notice that the reflection and transmission coefficients are defined as the ratios of the electric fields for TE waves and the ratios of the magnetic fields for TM waves, and their expressions are generally different.[31] The spectral reflectance and transmittance of the resonance cavity are calculated from the reflection and transmission coefficients as

$$R = rr^*, \tag{5}$$

$$T = \frac{\mathrm{Re}(n_i \cos\theta_s)}{\mathrm{Re}(n_s \cos\theta_i)} tt^* \quad \text{for TM waves}, \tag{6a}$$

$$T = \frac{\mathrm{Re}(n_s \cos\theta_s)}{\mathrm{Re}(n_i \cos\theta_i)} tt^* \quad \text{for TE waves}, \tag{6b}$$

where Re( ) takes the real part of a complex quantity, the asterisk denotes the complex conjugate, and n_i and n_s are the complex refractive indices of air and substrate, respectively.

[This article is copyrighted as indicated in the article. Reuse of AIP content is subject to the terms at: http://scitation.aip.org/termsconditions. Downloaded to] IP: 149.151.178.171 On: Thu, 24 Sep 2015 20:04:27

Using Eqs. (3) and (4), the square of the reflection and transmission coefficients can be expressed after simplifications as

$$rr^* = \frac{(\rho_a + \rho_s\zeta)^2 - 4\rho_a\rho_s\zeta \sin^2 \psi_1}{(1-\rho_a\rho_s)^2 + 4\rho_b\rho_s \sin^2 \psi_2}, \tag{7}$$

$$tt^* = \frac{\tau_a\tau_s}{(1-\rho_a\rho_s)^2 + 4\rho_b\rho_s \sin^2 \psi_2}, \tag{8}$$

where $\rho_a=|r_a|$, $\rho_b=|r_b|$, $\rho_s=|r_s|$, $\zeta=|t_at_b-r_ar_b|$, $\tau_a=t_at_a^*$, $\tau_s=t_st_s^*$, $\psi_1=(2\beta-\phi_a+\phi_s+\phi_\zeta)/2$, $\psi_2=(2\beta+\phi_b+\phi_s)/2$, $\phi_a=\arg(r_a)$, $\phi_b=\arg(r_b)$, $\phi_s=\arg(r_s)$, and $\phi_\zeta=\arg(r_\zeta)$. It should be noted that T represents the energy penetrating into the Ag reflector on the right and, thus, it will be eventually absorbed. In other words, the transmittance T represents the absorption by this Ag reflector. By examining the denominator of Eq. (8), it can be inferred that the maximum T occurs when the following condition is satisfied:

$$2\beta + \phi_b + \phi_s = 2m\pi, \tag{9}$$

where m is a positive integer. Here, ϕ's are the phase shifts due to the reflection from the corresponding boundary of the resonance cavity. Consequently, Eq. (9) states that the resonance occurs if total phase shifts in the cavity are multiples of 2π, where standing waves form in the cavity. On the other hand, the absorptance of the Fabry-Pérot cavity is $1-R$, where R is calculated from Eq. (7). The maximum absorptance (or minimum reflectance) occurs at frequencies slightly different from the one calculated with Eq. (9). However, the frequency shift is less than 10 cm^{-1}; hence, Eq. (9) is a good approximation of the resonance condition where the emissivity of the Fabry-Pérot cavity becomes the maximum.

Figure 7(a) shows the spectral-directional emissivity of the Fabry-Pérot cavity depicted in Fig. 1(b) for the near-IR spectral region at normal incidence. In the calculation, the cavity thickness is set to be 2.0 μm, and the Ag film on the right side of the cavity is assumed to be semi-infinite by setting its thickness much greater than the radiation penetration depth. The thickness of the front Ag film cannot be much greater than the radiation penetration depth to enable transmission of the incident wave into the cavity. In the present study, it was found that a 15 nm Ag film can maximize the emissivity peaks. In Fig. 7(a), the emissivity without the 15-nm-thick Ag film is also plotted for comparison. At the resonance frequency, where standing waves exist inside the cavity, very sharp emissivity peaks are found with the thin Ag film. The resonance features due to wave interference effects are clear from the fact that multiple emissivity peaks are found in the considered spectral region. Without the front Ag film, the resulting emissivity shows some oscillations, but the emissivity values are very low even at resonance frequencies. Therefore, high reflection from both boundaries of the cavity is the crucial factor to enable the large emissivity values. For Fabry-Pérot resonance cavities, the quality factor is defined as $Q=\Delta\nu/\delta\nu$ where $\Delta\nu$ is a free spectral range, which is the frequency difference between subsequent peaks, and is also called the *finesse*.[35] The definition of the quality factor is consistent with that of the PC-on-Ag structure by regarding that $\Delta\nu=\nu_c-0$, when only one

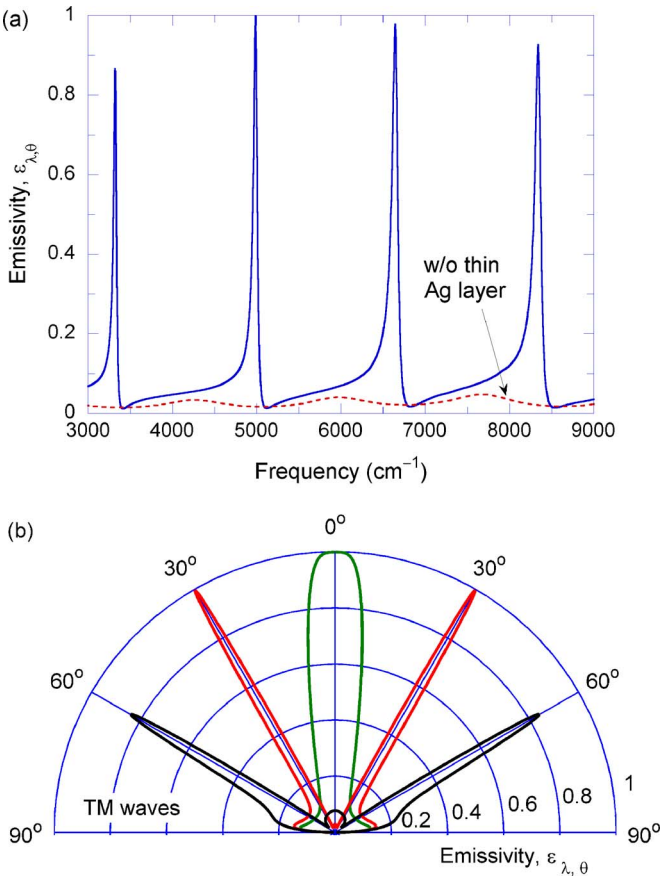

FIG. 7. (Color online) The emissivity $\varepsilon_{\lambda,\theta}$ of the Fabry-Pérot cavity: (a) spectral emissivity at normal incidence (solid line). The thickness of the SiO_2 cavity is 2 μm, and that of thin Ag film is 15 nm. The dotted line represents the case without a front Ag film. (b) Angular distribution of the emissivity at three peak frequencies for TM waves. The emissivity peaks corresponding to emission angles of $\theta=0°$, 30°, and 60° are centered at $\nu_c=4984.5$, 5284.0, and 6098.0 cm^{-1}, respectively.

peak is available like the case of the surface wave excitation. The quality factor of the Fabry-Pérot cavity near 5000 cm^{-1} is estimated as 28.6 at normal incidence. The low value of the quality factor is due to closely spaced emissivity peaks.

In order to demonstrate the spatial coherence of the Fabry-Pérot resonance cavity, the angular distribution of the spectral-directional emissivity is plotted in Fig. 7(b) at three peak frequencies around 5000 cm^{-1} for TM waves. The corresponding peak frequencies for emission angles of $\theta=0°$, 30°, and 60° are $\nu_c=4984.5$, 5284.0, and 6098.0 cm^{-1}, respectively. Unlike the PC-on-Ag structure, the normal emissivity is very close to unity, and the emissivity value decreases as the emission angle increases. The FWHM $\delta\theta$ of the angular lobes are estimated as 20.64°, 3.87°, and 6.09° for emission angles of 0°, 30°, and 60° respectively. These values are slightly smaller than those achieved from the PC-on-Ag structure. Since wave interference effects are independent of the polarization, the narrow angular lobes in the emissivity can also be found for TE waves at corresponding peak frequencies. However, for TE waves the peak frequencies at emission angles of 0°, 30°, and 60° are different from those for TM waves because the phase shifts ϕ_s and ϕ_b in Eq. (9) are based on reflection coefficients that depend on the

[This article is copyrighted as indicated in the article. Reuse of AIP content is subject to the terms at: http://scitation.aip.org/termsconditions. Downloaded to] IP: 149.151.178.171 On: Thu, 24 Sep 2015 20:04:27

polarization. The angular lobes of TE waves are found at $\nu_c = 5390.0$ and 6211.5 cm^{-1} for $\theta = 30°$ and 60°, respectively.

It would be interesting to investigate where the absorption occurs in the proposed structure because the Ag films on both sides of the dielectric can absorb the incident energy. From Eq. (8), the fraction of the absorption due to the right Ag reflector is approximately one-fourth, and thus, 75% of the absorbed energy is confined in the 15-nm-thick Ag film. From Kirchhoff's law, it can be thought that the 15-nm-thick Ag film contributes mostly to the thermal emission from the cavity. Note that the emissivity of a freestanding 15 nm Ag film is less than 0.1 near the frequency of 5000 cm^{-1}. Consequently, the dielectric cavity coated with highly reflective Ag films can significantly enhance thermal emission at the resonance frequencies and the emission is temporally and spatially coherent.

IV. EXPERIMENTAL RESULTS

To demonstrate the feasibility of the proposed structure as a coherent thermal emission source, we designed and fabricated the PC-on-Ag structure and the asymmetric Fabry-Pérot resonance cavity. The samples were fabricated using vacuum deposition techniques. A Si wafer of 100 mm diameter was used as the substrate for both structures. For the PC-on-Ag structure, a Ag film was coated up to 200 nm by sputtering deposition on the substrate with a thin Ti adhesive layer. Since the thickness of this Ag layer is much greater than the radiation penetration depth, the optical properties of Ti film and Si substrate do not affect the emissivity of the PC-on-Ag structure. The 1D PC with $\Lambda = 300$ nm was formed on top of the Ag layer using plasma enhanced chemical vapor deposition (PECVD). Both SiO_2 and Si_3N_4 were deposited at a temperature of 250 °C, and deposition processes of all layers were performed during one thermal cycle without breaking a vacuum environment; however, a 5 min nitrogen purge was applied in between the deposition of each layer to purge remaining chemical gases from the chamber.

The asymmetric Fabry-Pérot cavity was made in a similar manner. After depositing the 200-nm-thick Ag film on the Si substrate, SiO_2 was deposited using PECVD at 250 °C with the thickness of about 2 μm. Afterwards, approximately 15-nm-thick Ag film was sputtered atop the SiO_2. Once all fabrication processes were completed, the coated wafers were diced into 25.4×25.4 mm^2 specimens for the reflectance measurement.

The ABB Bomen FTLA 2000 series (MB154S) FTIR spectrometer measures the reflectance of the specimens at an incidence angle of 10° without polarization, using a specular reflectance accessory. The near-IR source is a quartz-halogen lamp with a tungsten filament, and the detector is a pyroelectric detector, which has an excellent linearity and can respond up to frequencies of 12 000 cm^{-1}. The stability of the near-IR source was examined over 3 h, and the output signal was found to be stable within 1% of fluctuation. A sample holder with an aperture of 9 mm diameter limited the beam size on the sample. The reflectance spectra were taken in the frequency range from 3000 to 12 000 cm^{-1} with a resolution of 2 cm^{-1}, with a Au mirror as the reference. The reflectance of the Au mirror was calculated using the optical constants from Ref. 32. The reflectance of each specimen was repeated ten times by interchanging the reference and the specimen, and each measurement was averaged over 64 scans. The background signal was measured without placing a sample, and the signal without sample (open aperture) was less than 0.5% of that with the Au mirror. The overall uncertainty of the measured reflectance is estimated to be 0.02, with a confidence interval of 95%, considering the instrument effects (such as beam divergence and alignment error), Au mirror reflectance, and repeatability.

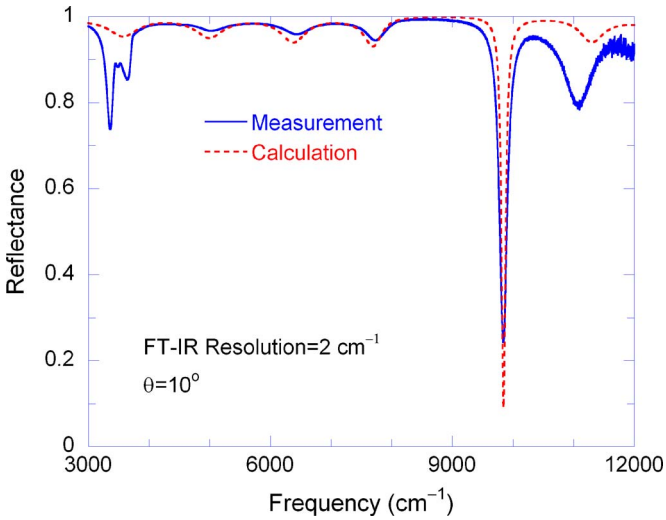

FIG. 8. (Color online) Spectral reflectance of the fabricated PC-on-Ag structure in the near-IR spectral region at room temperature. The solid and dashed lines represent the measured and predicted reflectance, respectively. The reflectance was measured by using the FTIR spectrometer with the resolution of 2 cm^{-1} at the angle of incidence 10°.

Figure 8 shows the measured and predicted reflectance of the PC-on-Ag structure. Since the reflectance spectrum is measured with the FTIR spectrometer, the reflectance rather than the emissivity is presented here. The solid line represents the mean value of the measurements, and the dashed line is from calculation. The difference in reflectance between TM and TE waves is negligibly small at the incidence angle of 10°. Therefore, the results can be considered as for either polarization or for unpolarized incidence. From Fig. 8, a very sharp reflectance dip can be seen near 10 000 cm^{-1}. Because the PC-on-Ag structure is essentially opaque, the decrease in the reflection is entirely due to the absorption by the structure. The FWHM $\delta\nu$ of the reflectance dip from the measurement is approximately 157 cm^{-1}. Therefore, the instrument resolution of 2 cm^{-1} is appropriate to resolve the abrupt drop in the reflectance of the PC-on-Ag structure.

At near normal incidence, the stop band of the 1D PC composed of SiO_2 and Si_3N_4 with $d_a = d_b$ and $\Lambda = 300$ nm is in the frequency range from 8800 to 10 600 cm^{-1}. Since actual thicknesses of dielectrics may slightly vary from the target value after deposition processes, Λ and a_1 are taken as fitting parameters to match the location of the reflectance dip. The best fitted values based on the resonance frequency are $\Lambda = 308$ nm and $a_1 = 0.655 d_a$. For the calculation here, the frequency-dependent optical constants of the dielectrics are used.[32] It should be noted that the thickness of the last Si_3N_4

[This article is copyrighted as indicated in the article. Reuse of AIP content is subject to the terms at: http://scitation.aip.org/termsconditions. Downloaded to] IP: 149.151.178.171 On: Thu, 24 Sep 2015 20:04:27

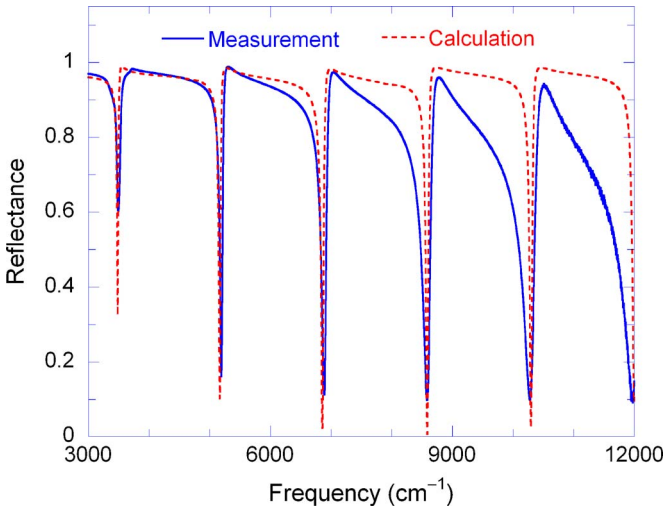

FIG. 9. (Color online) Spectral reflectance of the fabricated Fabry-Pérot cavity in the near-IR spectral region at room temperature. The solid and dashed lines represent the measured and predicted reflectance, respectively.

layer was 150 nm instead of 60 nm for the actual fabricated sample. This additional 90 nm dielectric layer affects the peak emissivity value slightly. It can be clearly seen that the calculated reflectance captures the essential features of the measured spectrum. The small reflectance dips found in the passband of the PC (e.g., at 6414 and 7727 cm^{-1}) are caused by wave interference effects in the multilayer structure and does not contribute much to the absorption. The slight difference between the measured and predicted reflectance is attributed to the impurities in dielectric films as well as the losses in Ag. Furthermore, the beam divergence of the FTIR spectrometer may cause some partial coherence inside the sample and also affect the measured reflectance spectrum.[30]

The measured reflectance of the Fabry-Pérot cavity is plotted in Fig. 9 together with the calculated. Several sharp reflectance dips exist with reflectance value close to 0.1. The free spectral range $\Delta\nu$ of the reflectance spectrum mainly depends on the refractive index and the thickness of the resonance cavity. By fitting $\Delta\nu$ and resonance frequencies, the thickness of the cavity is determined to be 1.968 μm, and the thickness of the front Ag film is found to be 22 nm. Reasonably good agreements are obtained between the measured and calculated reflectance. Compared to the PC-on-Ag structure, however, considerable deviations of the reflectance are found in the longer frequency range. Note that the optical constants in the deposited Ag film may not be exactly the same as those given in the handbook.

V. CONCLUSIONS

This work theoretically and experimentally demonstrates coherent thermal emission characteristics from two planar multilayer structures. One structure involves a truncated 1D PC with several unit cells coated on a polar material (SiC) or a metal (Ag). Coherent thermal emission can be achieved for both polarizations due to the excitation of surface waves at the interface between the 1D PC and SiC (or Ag). Coherent thermal emission is possible in the SiC phonon absorption band located at the mid-IR region, and the spectral region where coherent emission exists can be alternated to the near-IR region by replacing SiC with Ag. The other structure is the asymmetric Fabry-Pérot resonator made of the SiO_2 cavity coated with different-thickness Ag films on both sides. When standing waves exist inside the cavity, sharp spectral peaks and narrow angular lobes can be found in the spectral-directional emissivity. The thicker Ag layer mainly serves as a reflector, and the thinner Ag film in front of the dielectric layer contributes mostly to the emission of the structure. We have verified theoretical predictions by measuring the reflectance spectra of fabricated samples. The measured reflectance spectrum experimentally demonstrates coherence spectral characteristics in the PC-on-Ag structure, due to the excitation of surface waves in a planar multilayer without using a prism.

ACKNOWLEDGMENT

This work was supported by the National Science Foundation (CTS-0500113).

[1]R. Siegel and J. R. Howell, *Thermal Radiation Heat Transfer*, 4th ed. (Taylor & Francis, New York, 2002).
[2]P. J. Hesketh, J. N. Zemel, and B. Gebhart, Nature (London) **324**, 549 (1986).
[3]J.-J. Greffet, R. Carminati, K. Joulain, J.-P. Mulet, S. Mainguy, and Y. Chen, Nature (London) **416**, 61 (2002).
[4]F. Marquier, K. Joulain, J.-P. Mulet, R. Carminati, J.-J. Greffet, and Y. Chen, Phys. Rev. B **69**, 155412 (2004).
[5]A. Boueke, R. Kühn, P. Fath, G. Willeke, and E. Bucher, Sol. Energy Mater. Sol. Cells **65**, 549 (2001).
[6]T. J. Coutts, Renewable Sustainable Energy Rev. **3**, 77 (1999).
[7]M. Kreiter, J. Oster, R. Sambles, S. Herminghaus, S. Mittler-Neher, and W. Knoll, Opt. Commun. **168**, 117 (1999).
[8]H. Raether, *Surface Plasmons on Smooth and Rough Surfaces and on Gratings* (Springer-Verlag, Berlin, 1988).
[9]R. A. Shelby, D. R. Smith, and S. Schultz, Science **292**, 77 (2001).
[10]C. J. Fu, Z. M. Zhang, and D. B. Tanner, Opt. Lett. **30**, 1873 (2005).
[11]B. J. Lee, C. J. Fu, and Z. M. Zhang, Appl. Phys. Lett. **87**, 071904 (2005).
[12]B. J. Lee and Z. M. Zhang, J. Heat Transfer (to be published).
[13]E. F. Schubert, N. E. J. Hunt, A. M. Vredenberg, T. D. Harris, J. M. Poate, D. C. Jacobson, Y. H. Wong, and G. J. Zydzik, Appl. Phys. Lett. **63**, 2603 (1993).
[14]O. G. Kollyukh, A. I. Liptuga, V. Morozhenko, and V. I. Pipa, Opt. Commun. **225**, 349 (2003).
[15]P. Ben-Abdallah, J. Opt. Soc. Am. A **21**, 1368 (2004).
[16]P. Ben-Abdallah and B. Ni, J. Appl. Phys. **97**, 104910 (2005).
[17]I. Celanovic, D. Perreault, and J. Kassakian, Phys. Rev. B **72**, 075127 (2005).
[18]A. Narayanaswamy and G. Chen, Phys. Rev. B **70**, 125101 (2004).
[19]L. Dal Negro, J. H. Yi, V. Nguyen, Y. Yi, J. Michel, and L. C. Kimerling, Appl. Phys. Lett. **86**, 261905 (2005).
[20]J. A. Gaspar-Armenta and F. Villa, J. Opt. Soc. Am. B **20**, 2349 (2003).
[21]W. M. Robertson and M. S. May, Appl. Phys. Lett. **74**, 1800 (1999).
[22]P. Yeh, A. Yariv, and C. S. Hong, J. Opt. Soc. Am. **67**, 423 (1977).
[23]J. A. Gaspar-Armenta and F. Villa, J. Opt. Soc. Am. B **21**, 405 (2004).
[24]M. Laroche, R. Carminati, and J.-J. Greffet, Phys. Rev. Lett. **96**, 123903 (2006).
[25]H. Sai, Y. Kanamori, and H. Yugami, Appl. Phys. Lett. **82**, 1685 (2003).
[26]C. H. Seager, M. B. Sinclair, and J. G. Fleming, Appl. Phys. Lett. **86**, 244105 (2005).
[27]S. Bauer, Am. J. Phys. **60**, 257 (1992).
[28]M. Laroche, F. Marquier, R. Carminati, and J.-J. Greffet, Opt. Commun. **250**, 316 (2005).
[29]J. D. Joannopoulos, R. D. Meade, and J. N. Winn, *Photonic Crystals* (Princeton University Press, Princeton, NJ, 1995).
[30]Z. M. Zhang, C. J. Fu, and Q. Z. Zhu, Adv. Heat Transfer **37**, 179 (2003).

[This article is copyrighted as indicated in the article. Reuse of AIP content is subject to the terms at: http://scitation.aip.org/termsconditions. Downloaded to] IP: 149.151.178.171 On: Thu, 24 Sep 2015 20:04:27

[31]M. Born and E. Wolf, *Principles of Optics*, 7th ed. (Cambridge University Press, Cambridge, UK, 1999).
[32]E. D. Palik, *Handbook of Optical Constants of Solids I & II* (Academic, San Diego, CA, 1998).
[33]F. Ramos-Mendieta and P. Halevi, J. Opt. Soc. Am. B **14**, 370 (1997).
[34]W. M. Robertson, J. Lightwave Technol. **17**, 2013 (1999).
[35]J. M. Vaughan, *The Fabry-Perot Interferometer* (Adam Hilger, Philadelphia, PA, 1989).

[This article is copyrighted as indicated in the article. Reuse of AIP content is subject to the terms at: http://scitation.aip.org/termsconditions. Downloaded to] IP: 149.151.178.171 On: Thu, 24 Sep 2015 20:04:27